Effective mass of heavy, light, and spin split-off band electron and hole g-factor in cubic perovskite materials

Ompong, David; Inkoom, Godfred; Singh, Jai

Published in:
Journal of Applied Physics

DOI:
10.1063/5.0028266

Published: 21/12/2020

Document Version
Peer reviewed version

Effective mass of heavy, light, and spin split-off band electron and hole g-factor in cubic perovskite materials

David Ompong[1], Godfred Inkoom[2] and Jai Singh[1a]

[1]*College of Engineering, IT and Environment, Charles Darwin University, Darwin, NT , 0909, Australia*

[2]*Department of Physics & Astronomy, Mississippi State University, Starkville, MS, 39762-5167, USA*

[a] Corresponding author: jai.singh@cdu.edu.au

Abstract

Analytical expressions for the effective mass of heavy, light, and spin split-off electrons are obtained by diagonalizing the $\boldsymbol{k}\cdot\boldsymbol{p}$ Hamiltonian for cubic perovskite crystal structures and used to calculate these in nine perovskite materials. An expression for the effective hole g-factor is also derived and calculated in these perovskites. The calculated effective mass of heavy electron ranges from $1.619m_0$ to $0.201m_0$, of light electron from $0.357m_0$ to $0.146m_0$, and of spin split-off electron from $0.584m_0$ to $0.169m_0$. It is found that Cl- and Pb-based perovskite materials have larger heavy, light and spin split-off electron effective masses. It is also found that the effective g-factor increases with the atomic size, from Cl to I, for the series $CsSnX_3 (X = Cl, Br, I)$.

I. INTRODUCTION

Theoretical and experimental works on semiconductors such as Si, Ge, GaAs, and InSb under stress have provided useful insight and detailed understanding of their band structures [1]. On the theory side, $\boldsymbol{k}\cdot\boldsymbol{p}$ method has been very useful for studying the energy band structures and physical phenomena occurring near the center of the Brillouin zone (BZ) of semiconductors [1-3]. Recently, perovskite semiconductors have been used in several applications, for example, in solar cells, lasers, photo-rechargeable batteries, and light emitting diodes (LEDs) [3-7]. The $\boldsymbol{k}\cdot\boldsymbol{p}$

method has also been used to study the electronic and optical properties of perovskites without including the effect of charge carrier scattering by optical phonons [3, 8]. The finding of large effective masses along some principal axes in perovskite materials have been reported as anomalies [8]. Density functional theory and quasi particle self-consistent GW electronic structure calculations have been used to study the electronic transport properties in halide cubic perovskites $CsSnX_3(X = Cl, Br, I)$ [9] and it has been found that by increasing X results in deceasing the effective masses of heavy and light electrons in the conduction band (CB) along the [100] and [111] directions. As the electron mobility (μ) and effective mass (m_e) are related by $\mu = \frac{e\tau}{m_e}$, where e is the electronic charge and τ is the electron scattering time, any change in the effective mass of an electron is expected to influence the mobility, which in turn affects the optoelectronic properties of perovskite devices [9-11]. As a result, a semiconductor with anisotropic electron effective mass will have anisotropic mobility leading to anisotropic charge density [11-14]. Therefore, effective mass and band gap energy are among the most important parameters needed to characterise any semiconductor material.

The effective mass of an electron in the CB at a point $\mathbf{k} = \mathbf{k}_0$ is given by, $\frac{\hbar^2}{\left(\frac{\partial^2 E(k)}{\partial k^2}\right)\Big|_{\mathbf{k}=\mathbf{k}_0}}$, where $\hbar = h/2\pi$ is the reduced Planck's constant and $E(k)$ is the electron energy obtained from the dispersion relation at wavevector k, and hence it depends on the electronic band structure [15]. It has been established that the presence of mechanical strain and spin-orbit coupling (SOC) can reduce the crystal symmetry [1], and split the electronic energy bands. However, in perovskites, the splitting of the conduction band due to strain field is found to be relatively small compared to that due to the SOC [3]. The magnitude of the strain field is not given here because the influence of hydrostatic, uniaxial, and shear strain on the unstrained crystal potential and their effects on the optoelectronic properties [2, 3] of perovskite heterostructures will be considered in a future study. Using band theory calculation including the electron-electron interaction and

SOC, it is found that the holes in the valence band of perovskite materials have angular momentum eigenvalue $J = \frac{1}{2}$, whereas the electrons in the conduction band have eigenvalue $J = \frac{3}{2}$. This is similar but opposite to the case of electrons and holes in many III-V semiconductors, where the holes have $J = \frac{3}{2}$ and electron has $J = \frac{1}{2}$ [4]. In perovskite materials, the vectorial representation of the conduction band minimum at R-point splits into spin-split off (SO), light electron (LE) and heavy electron (HE) electron bands [16-18]. A schematic band structure of perovskite materials is shown in Figure 1. However, such a splitting does not occur in the valence band and hence the valence band is degenerate, isotropic and parabolic [9]. To our knowledge, this is the first theoretical study of the effective mass of the heavy, light, and spin split-off electrons, and effective g-factor of holes in perovskite materials.

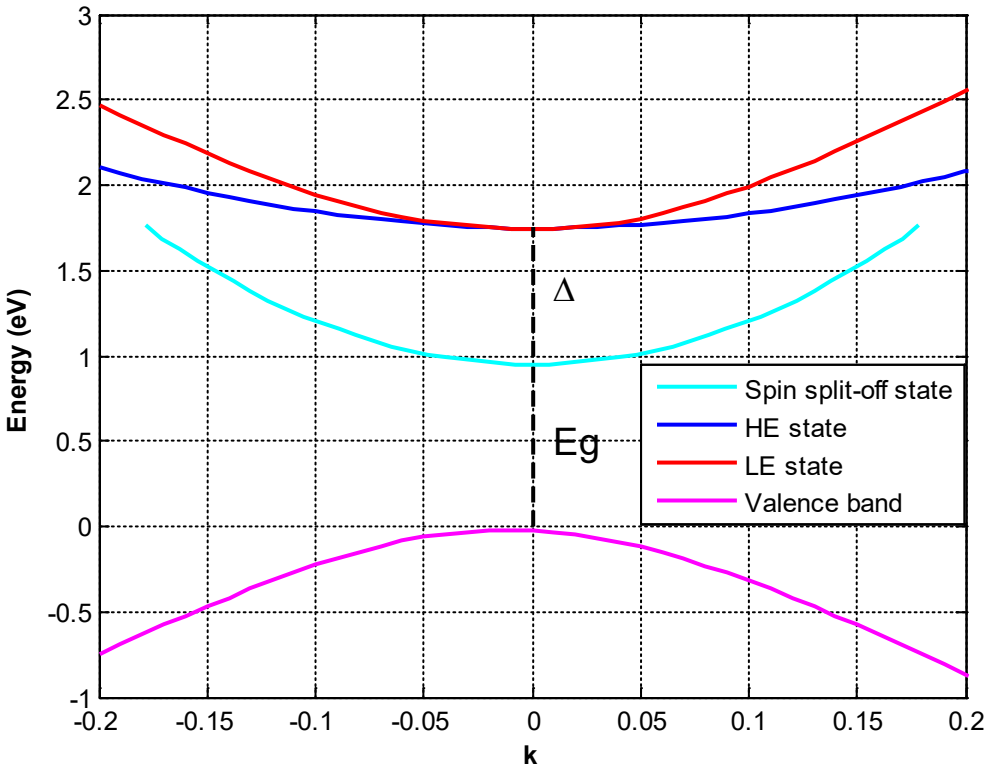

FIG. 1. Schematic band structure of the valence and conduction bands in perovskite materials.

In this paper, we have first derived analytical expressions for the effective mass of heavy, light, and spin split-off electrons and effective g-factor of holes in cubic perovskite materials for the first time. We have diagonalized the 8x8 matrix Hamiltonian for cubic perovskite structure with direct band gap at the R-point to obtain the analytical expressions, which are then used to calculate the electron effective masses for some inorganic and hybrid organic cubic perovskite materials and effective g-factors of holes. The results of this study may be useful in the design of perovskite-based devices.

II. ELECTRON EFFECTIVE MASS IN CUBIC PEROVSKITE MATERIALS

Luttinger[19] developed the quantum theory of cyclotron resonance using a four-band model, for semiconductors with diamond structure. Pidgeon and Brown[20] extended the four-band model to eight-band model by considering the conduction band together with the degenerate valence band. Accordingly, the band structure of a bulk cubic perovskite semiconductors material at the R-point can be described by an 8x8 matrix Hamiltonian $\widehat{H}$[17, 21] given in Table I. The fully coupled Hamiltonian includes double spin-degenerate *p*-like orbitals of the conduction band HE, LE, and SO bands and *s*-like orbitals of the valence band.

Table I. Matrix Hamiltonian $\widehat{H}$ representing the cubic perovskite structure with direct band gap at the R-point [17].

	$\lvert S\uparrow\rangle$	$\lvert S\downarrow\rangle$	$\left\lvert\frac{3}{2}\ \frac{3}{2}\right\rangle$	$\left\lvert\frac{3}{2}\ \frac{1}{2}\right\rangle$	$\left\lvert\frac{3}{2}-\frac{1}{2}\right\rangle$	$\left\lvert\frac{3}{2}-\frac{3}{2}\right\rangle$	$\left\lvert\frac{1}{2}\ \frac{1}{2}\right\rangle$	$\left\lvert\frac{1}{2}-\frac{1}{2}\right\rangle$
$\langle S\uparrow\rvert$	VB	0	$\frac{1}{\sqrt{2}}P_+$	$-\frac{\sqrt{2}}{\sqrt{3}}P_z$	$-\frac{1}{\sqrt{6}}P_-$	0	$-\frac{1}{\sqrt{3}}P_z$	$-\frac{1}{\sqrt{3}}P_-$
$\langle S\downarrow\rvert$	0	VB	0	$\frac{1}{\sqrt{6}}P_+$	$-\frac{\sqrt{2}}{\sqrt{3}}P_z$	$-\frac{1}{\sqrt{2}}P_-$	$-\frac{1}{\sqrt{3}}P_+$	$\frac{1}{\sqrt{3}}P_z$

$\left\langle \frac{3}{2}\ \frac{3}{2}\right\vert$	$\frac{1}{\sqrt{2}}P_-$	0	CH	S	$-R$	0	$\frac{S}{\sqrt{2}}$	$-\sqrt{2}R$
$\left\langle \frac{3}{2}\ \frac{1}{2}\right\vert$	$-\frac{\sqrt{2}}{\sqrt{3}}P_z$	$-\frac{1}{\sqrt{6}}P_-$	S^*	CL	0	$-R$	$-D$	$\frac{\sqrt{3}}{\sqrt{2}}S$
$\left\langle \frac{3}{2}-\frac{1}{2}\right\vert$	$-\frac{1}{\sqrt{6}}P_+$	$-\frac{\sqrt{2}}{\sqrt{3}}P_z$	$-R^*$	0	CL	$-S$	$-\frac{\sqrt{3}}{\sqrt{2}}S^*$	D
$\left\langle \frac{3}{2}-\frac{3}{2}\right\vert$	0	$-\frac{1}{\sqrt{2}}P_+$	0	$-R^*$	$-S^*$	CH	$\sqrt{2}R^*$	$\frac{1}{\sqrt{2}}S^*$
$\left\langle \frac{1}{2}\ \frac{1}{2}\right\vert$	$-\frac{1}{\sqrt{3}}P_z$	$-\frac{1}{\sqrt{3}}P_-$	$\frac{1}{\sqrt{2}}S^*$	$-D$	$-\frac{\sqrt{3}}{\sqrt{2}}S$	$\sqrt{2}R$	CS	0
$\left\langle \frac{1}{2}-\frac{1}{2}\right\vert$	$-\frac{1}{\sqrt{3}}P_+$	$\frac{1}{\sqrt{3}}P_z$	$-\sqrt{2}R^*$	$-\frac{\sqrt{3}}{\sqrt{2}}S^*$	D	$\frac{1}{\sqrt{2}}S$	0	CS

where

$$P_{\pm} = P\left(k_x \pm ik_y\right) \tag{1}$$

$$P_z = Pk_z + i\delta \tag{2}$$

$$VB = E_G + \frac{\hbar^2}{2m_0}\gamma_v\left[k_x^2 + k_y^2 + k_z^2\right] \tag{3}$$

$$\gamma_v = \frac{1}{m_h} - \frac{E_p}{3}\left(\frac{2}{E_G} + \frac{1}{E_G + \Delta}\right) \tag{4}$$

$$CH = \frac{\hbar^2}{2m_0}\left[(\gamma_1 + \gamma_2)\left(k_x^2 + k_y^2\right) + (\gamma_1 - 2\gamma_2)k_z^2\right] \tag{5}$$

$$CL = \frac{\hbar^2}{2m_0}\left[(\gamma_1 - \gamma_2)\left(k_x^2 + k_y^2\right) + (\gamma_1 + 2\gamma_2)k_z^2\right] \tag{6}$$

$$CS = \frac{\hbar^2}{2m_0}\left[\gamma_1\left(k_x^2 + k_y^2 + k_z^2\right)\right] - \Delta \tag{7}$$

$$S = \frac{\hbar^2}{2m_0} 2\sqrt{3}\,\gamma_3\left(-k_x + ik_y\right)k_z \tag{8}$$

$$R = \frac{\hbar^2}{2m_0}\sqrt{3}\left[\gamma_2\left(k_x^2 - k_y^2\right) - 2i\gamma_3 k_x k_y\right] \tag{9}$$

$$D = \frac{\hbar^2}{2m_0}\sqrt{2}\gamma_2\left(k_x^2 + k_y^2 - 2k_z^2\right) \tag{10}$$

$$E_p = \frac{2m_0}{\hbar^2}P^2 = \frac{2}{m_0}P_0^2 \tag{11}$$

$$P = -i\frac{\hbar}{m_0} < s|p_x|x > \tag{12}$$

$$p_x = -i\hbar\frac{\partial}{\partial x} \tag{13}$$

In Table I, $|S\uparrow\rangle$ and $|S\downarrow\rangle$ represent the valence hole states, $\left|\frac{3}{2}\ \pm\frac{3}{2}\right\rangle$ and $\left|\frac{3}{2}\pm\ \frac{1}{2}\right\rangle$ represent the four-fold degenerate heavy and light electron states, and $\left|\frac{1}{2}\ \frac{1}{2}\right\rangle$ and $\left|\frac{1}{2}-\frac{1}{2}\right\rangle$ represent spin split-off electron in the conduction band. The 8x8 matrix Hamiltonian cannot be block diagonalized completely for any arbitrary *k,* however, the matrix elements in the Hamiltonian (Table I) can be diagonalized analytically if we consider only small *k* values [2, 13], which makes the inter-band matrix elements negligible in comparison with SO coupling. Then the 8x8 matrix Hamiltonian can be partitioned into three intra-band matrices: (1) a 2x2 valence band matrix Hamiltonian (includes first 2 columns and first two rows of Table I), (2) a 4x4 matrix Hamiltonian for HE and LE electrons in the conduction band as given in Table II, and (3) a 2x 2 matrix Hamiltonian for the spin split-off electrons in the conduction band as given in Table III. Finally, to derive the effective mass of the heavy and light electrons, we diagonalize the 4 x 4 matrix given in Table II.

Table II. Matrix Hamiltonian for calculating the effective mass of heavy and light electrons in the conduction band.

	$\left\vert\frac{3}{2}\ \frac{3}{2}\right\rangle$	$\left\vert\frac{3}{2}\ \frac{1}{2}\right\rangle$	$\left\vert\frac{3}{2}\ -\frac{1}{2}\right\rangle$	$\left\vert\frac{3}{2}\ -\frac{3}{2}\right\rangle$
$\left\langle\frac{3}{2}\ \frac{3}{2}\right\vert$	CH	S	$-R$	0
$\left\langle\frac{3}{2}\ \frac{1}{2}\right\vert$	S^*	CL	0	$-R$
$\left\langle\frac{3}{2}\ -\frac{1}{2}\right\vert$	$-R^*$	0	CL	$-S$
$\left\langle\frac{3}{2}\ -\frac{3}{2}\right\vert$	0	$-R^*$	$-S^*$	CH

Table III. Matrix Hamiltonian for deriving the effective mass of spin split-off electron in the conduction band.

	$\left\vert\frac{1}{2}\ \frac{1}{2}\right\rangle$	$\left\vert\frac{1}{2}\ -\frac{1}{2}\right\rangle$
$\left\langle\frac{1}{2}\ \frac{1}{2}\right\vert$	CS	0
$\left\langle\frac{1}{2}\ -\frac{1}{2}\right\vert$	0	CS

By diagonalizing and solving the eigenvalue of the matrix $|H\text{-}E(k)| = 0$ in Table II, we get the energy eigenvalue for heavy and light electrons as:

$$E(k) = \left(\frac{\hbar^2}{2m_0}\right)\Big\{\gamma_1 k^2 \pm 2\big(\gamma_2^2\big[k_x^2\big(k_x^2 - k_y^2\big) + k_y^2\big(k_y^2 - k_z^2\big) + k_z^2\big(k_z^2 - k_x^2\big) + 3\gamma_3^2\big(k_x^2 k_y^2 + k_y^2 k_z^2 + k_z^2 k_x^2\big)\big]\big)^{\frac{1}{2}}\Big\} \quad (14)$$

where $k^2 = k_x^2 + k_y^2 + k_z^2$, m_0 is the free electron mass and + and – signs in the second term within the bracket are assigned to represent the light and heavy electrons, respectively. In Eq. (14), the normalised Luttinger parameters[17], γ_i $[i = 1,2,3]$ are the linearly independent parameters which determine the curvature of the energy band away from the R-point. Eq. (14) is anisotropic unless $\gamma_3 = 0$ and non-parabolic unless both $\gamma_{2,3} = 0$. Equating $E(k)$ on the left hand side of Eq. (14) with the energy of the electron obtained within the effective mass approximation:

$$E(k) = \frac{\hbar^2 k^2}{2m_{\pm e}} \quad (15)$$

we get:

$$\frac{m_0}{m_{\pm e}} = \left\{\gamma_1 \pm \frac{2}{k^2}\big(\gamma_2^2\big[k_x^2\big(k_x^2 - k_y^2\big) + k_y^2\big(k_y^2 - k_z^2\big) + k_z^2\big(k_z^2 - k_x^2\big) + 3\gamma_3^2\big(k_x^2 k_y^2 + k_y^2 k_z^2 + k_z^2 k_x^2\big)\big]\big)^{\frac{1}{2}}\right\} \quad (16)$$

where $m_{+e} = m_{le}$ and $m_{-e} = m_{he}$ represent the light and heavy electron masses, respectively. From Eq. (16), we can express the effective masses of the heavy and light electrons in the [110] $\big(k_x = k_y = 1, k_z = 0\big)$ direction as:

$$m_{he}[110] = \left(\gamma_1 - \sqrt{\gamma_2^2 + 3\gamma_3^2}\right)^{-1} m_0 \quad (17a)$$

and

$$m_{le}[110] = \left(\gamma_1 + \sqrt{\gamma_2^2 + 3\gamma_3^2}\right)^{-1} m_0 \qquad (17b)$$

Likewise, to derive the effective mass of the spin split-off electron we diagonalize the 2 x 2 matrix in Table III and solve $|H - E_{SO}(k)| = 0$, which gives:

$$E_{SO}(k) = CS = \frac{\hbar^2}{2m_0}\left[\gamma_1\left(k_x^2 + k_y^2 + k_z^2\right)\right] - \Delta \qquad (18)$$

and then applying the effective mass approximation by writing:

$$E_{SO}(k) = \frac{\hbar^2 k^2}{2m_{so}} \qquad (19)$$

and equating with Eq. (18), we get the effective mass of the spin split-off electron m_{so} in the conduction band as:

$$\frac{m_0}{m_{so}} = \gamma_1 - \frac{2m_0\Delta}{\hbar^2 k^2} \qquad (20)$$

where Δ is the SOC splitting in the CB.

For calculating the effective mass of electrons in the heavy and light from Eq. (16) and spin split-off from Eq. (20) bands, one requires the input parameters which are listed in Table IV for all inorganic and hybrid organic-inorganic perovskite materials known to have cubic crystal structure. Some of these parameters are extracted from published figures as described below: The band gap (E_g) and spin-orbit splitting (Δ) energies for the first three materials, $CsPbX_3 (X = Cl, Br, I)$, in Table IV are obtained from ref. 18 (extracted from Figure 1b in the text and the Extended Data Figure 1 in the section methods). For the next three materials, $CsSnX_3 (X = Cl, Br, I)$, E_g and Δ are obtained from ref. 9 (E_g is given in Table IV

and Δ in Table III of ref. 9). The effective mass of valence band hole (m_h) and Kane energy (E_P) for $CsPbX_3 (X = Cl, Br, I)$ are obtained from the supplementary information (TABLE S1) of ref. 18 and the lattice constant (a) are given under Band-structure calculations on the right column of page 194 of ref. 18. For the next three materials, $CsSnX_3 (X = Cl, Br, I)$, we have calculated E_P from the method described in section 1b of the supplementary text of ref. 18 and the values of Δ, m_h and a are given in TABLE III, Table VI, and Table I, respectively, of ref. 9.

The Luttinger parameters in table IV are calculated as follows: Eqs.(7a)-(7d) in ref. 17 relate the Luttinger parameters with the effective masses in the [100] and [111] directions which are in turn related to the inverse mass parameters, A, B and C in Eqs.(2) and (3) of ref 9. Therefore, γ_1^L, γ_2^L and γ_3^L are calculated from the known A, B and C for all the 9 cubic perovskites as:

$$\gamma_1^{\mathrm{L}} = \frac{1}{2}(\mathrm{A} + \mathrm{B}) \tag{21}$$

$$\gamma_2^{\mathrm{L}} = \frac{1}{4}(\mathrm{A} - \mathrm{B}) \tag{22}$$

$$\gamma_3^{\mathrm{L}} = \frac{1}{4}\mathrm{C} \tag{23}$$

Using Eqs. (21)-(23), the normalized Luttinger parameters $\gamma_1, \gamma_2, \gamma_3$ are obtained as[17]:

$$\gamma_1 = \gamma_1^L - \frac{1}{3}\frac{E_P}{E_{\mathrm{g}}} \tag{24}$$

$$\gamma_2 = \gamma_2^L - \frac{1}{6}\frac{E_P}{E_{\mathrm{g}}} \tag{25}$$

$$\gamma_3 = \gamma_3^L - \frac{1}{6}\frac{E_P}{E_{\mathrm{g}}} \tag{26}$$

Using Eqs. (24) – (26), the effective masses can be calculated from Eqs. (16) and (20). As explained above, all the parameters in Table IV are calculated theoretically and obtained from references shown in Table IV, except the band gap energies listed in the column 3, which are experimental values. As the experimental E_g is known only for four materials (see Table IV), we have used the theoretical values known for all the materials. However, according to Table IV, the experimental and theoretical values of E_g are in reasonable agreement.

Table IV: Input parameters for calculating the effective masses of spin split-off, heavy and light electrons and effective g-factor of holes in perovskite materials.

	E_g^{theo} (eV)	E_g^{exp} (eV)	Δ(eV)	γ_1^L	γ_2^L	γ_3^L	$m_h(m_0)$	E_P(eV)	a(Å)
$CsPbCl_3$	3.27[a]	3.04[e]	1.53[a]	5.8	2.2	0.5	0.170[a]	40.1[a]	5.610[a]
$CsPbBr_3$	2.36[a]	2.36[e]	1.50[a]	7.6	3.0	0.7	0.128[a]	39.9[a]	5.865[a]
$CsPbI_3$	2.05[a]	1.73[f]	1.44[a]	9.1	3.6	0.7	0.095[a]	41.6[a]	6.238[a]
$CsSnCl_3$	2.69[b]	_	0.45[b]	6.4	2.5	0.8	0.140[b]	34.7	5.560[b]
$CsSnBr_3$	1.38[b]	_	0.44[b]	10.2	4.3	1.7	0.082[b]	35.7	5.804[b]
$CsSnI_3$	1.01[b]	_	0.42[b]	13.0	5.6	2.1	0.069[b]	29.9	6.219[b]
$CH_3NH_3PbI_3$	1.60[c]	1.57[f]	1.40	_	_	_	0.170[h]	15.3[c]	6.200[f]
$CsSiI_3$	0.31[d]	_	0.50	24.3	11.5	8.1	_	18.9	5.892[d]
$CsGeI_3$	1.20[d]	_	0.27	11.4	5.0	1.4	_	28.2	6.050[d]

a=18,b=9, c=22, d=5, e=23,f=24, g=17, h=3.

III. HOLE EFFECTIVE g-FACTOR IN CUBIC PEROVSKITE MATERIALS

The effective g-factor for the s-like hole, $g^* = g_0 + g'$, where g' is derived from second-order perturbation theory as[2]:

$$g' = \frac{g_0}{im_0}\sum_{\alpha}\frac{\langle S\uparrow|p_x|\alpha\rangle\langle\alpha|p_y|S\uparrow\rangle - \langle S\uparrow|p_y|\alpha\rangle\langle\alpha|p_x|S\uparrow\rangle}{E_S - E_\alpha} \tag{27}$$

We assume that the only relevant states to be included in the summation in Eq. (27) are from the heavy, light and spin split-off states of the conduction band as listed in Table V.

TABLE V. Matrix elements of the heavy (he), light (le) and spin split-off (so) states for computing g'in cubic crystal perovskite materials from Eq. (27).

	$\langle iS\uparrow\|p_x\|\alpha\rangle$	$\langle\alpha\|p_x\|iS\uparrow\rangle$	$\langle iS\uparrow\|p_y\|\alpha\rangle$	$\langle\alpha\|p_y\|iS\uparrow\rangle$
$he\uparrow$	$\frac{1}{\sqrt{2}}P_0$	$\frac{1}{\sqrt{2}}P_0$	$i\frac{1}{\sqrt{2}}P_0$	$i\frac{1}{\sqrt{2}}P_0$
$he\downarrow$	0	0	0	0
$le\uparrow$	0	0	0	0
$le\downarrow$	$-\frac{1}{\sqrt{6}}P_0$	$-\frac{1}{\sqrt{6}}P_0$	$i\frac{1}{\sqrt{6}}P_0$	$i\frac{1}{\sqrt{6}}P_0$
$se\uparrow$	0	0	0	0
$se\downarrow$	$-\frac{1}{\sqrt{3}}P_0$	$-\frac{1}{\sqrt{3}}P_0$	$i\frac{1}{\sqrt{3}}P_0$	$i\frac{1}{\sqrt{3}}P_0$

Using Table V in Eq. (27), we obtain:

$$g' = \frac{g_0 E_P \Delta}{3E_g(E_g + \Delta)} \tag{28}$$

It may be noted that according to Eqs. (27) and (28), the effective g-factor $g^* \neq g_0$ only if the spin-orbit interaction Δ is non-zero.

IV. RESULTS AND DISCUSSIONS

We have presented the derivations of the effective masses of heavy-, light- (in Eq. (16)), and spin split-off- (in Eq. (20)) electrons and effective g-factor of holes in perovskite materials. The calculated effective masses from Eqs. (16) and (20) and the effective g-factor g^* from Eq. (27) are listed in Table VI along with the magnitude of experimental g-factor of holes in two perovskite materials. The Luttinger parameters $\gamma_i^L (i = 1,2,3)$ required to calculate the effective masses from Eqs. (16) and (20) were calculated using the inverse mass parameters *A*, *B*, and *C* of the Kohn-Luttinger Hamiltonian [9] [17], and are listed in Table IV. The *A*, *B*, and *C* of $CsSnX_3 (X = Cl, Br, I)$ are listed in TABLE VII in ref 9. It may be noted that the Luttinger-Kohn parameters for the perovskite $CH_3NH_3PbI_3$ are not known and hence $\gamma_i^L (i = 1,2,3)$ for this perovskite could not be calculated. As $CsPbI_3$ and $CH_3NH_3PbI_3$ have only Cs and CH_3NH_3 different in their structures, we have assumed that the Luttinger parameters for $CH_3NH_3PbI_3$ are the same as for $CsPbI_3$ in our calculations.

It may be desirable to point out that although perovskite materials may exist in three phases; orthorhombic(γ-phase), tetragonal(β-phase) and cubic(α-phase), many of them hold their stable structure in the γ -phase [5]. We have not considered β- and γ- phases here, as the high temperature cubic structure of perovskite materials may be regarded to be an ideal structure to understand the basic properties of perovskites [3]. The cubic perovskite materials have smaller effective masses compared with the orthorhombic and tetragonal structures [8], therefore, we expect the effective masses of the β- and γ- structures to be larger than the values in Table VI.

It is evident from Table VI that as the atomic size of the halide atom X increases from Cl to I, the effective mass of the heavy, light and spin split-off electrons decreases. The perovskite with Pb (Ge) of larger atomic size has heavier effective mass than that with Sn (Si) of smaller atomic

size. Our results agree with previously simulated effective masses in perovskite materials [8]. It may also be noted that the Luttinger parameters of Cl- based perovskite materials shown in Table IV are consistently smaller than their Br- and I-based counterparts and that of Pb-based perovskite materials are also consistently smaller than their Sn-based counterparts. This establishes a clear inverse relation between the effective mass and the Luttinger parameters of metal halide perovskites.

Table VI: Effective masses of heavy electron (m_{he}), light electron (m_{le}), split-off electron (m_{so}), and effective g-factors of holes, calculated using Eq. (14), (16), and $g^* = g_0 + g'$. The input values for the calculation are given in Table IV.

	$m_{he}(m_0)$	$m_{le}(m_0)$	$m_{so}(m_0)$	$g^{*theo}(g_0)$	$g^{*exp}(g_0)$
$CsPbCl_3$	1.619	0.357	0.584	1.23	_
$CsPbBr_3$	1.605	0.303	0.509	1.60	0.75 [25]
$CsPbI_3$	1.367	0.254	0.428	1.90	_
$CsSnCl_3$	0.687	0.298	0.415	0.77	_
CsSnBr3	0.682	0.247	0.362	1.30	_
$CsSnI_3$	0.672	0.210	0.319	1.75	_
$CH_3NH_3PbI_3$	0.201	0.146	0.169	1.24	0.41 [26]

$CsSiI_3$	0.378	0.189	0.251	6.77	
$CsGeI_3$	0.486	0.197	0.280	1.22	

In Table VI, we see that g' in Eq (28) depends on bandgap energy E_g, spin-orbit splitting energy Δ, and the Kane energy E_P. Although the expression of g' in Eq (28) is the same as the one found for the zinc-blende semiconductors [2, 13], g' is positive in perovskite materials and negative in zinc-blende semiconductors. The calculated values of the g-factor could be compared with their known experimental values only for $CsPbBr_3$ and $CH_3NH_3PbI_3$, the calculated values are about twice the experimental results. We observe that an increase in atomic size from Cl to I for the series $CsSnX_3 (X = Cl, Br, I)$ results in an increase in the effective g-factor. We have also found (see Table VI), that the effective g-factor of $CsSiI_3$ is the largest which is due to the small bandgap E_g in the denominator of Eq. (28).

V. CONCLUSIONS

We have derived expressions for the effective mass of heavy, light, spin split-off electrons and effective g-factor of holes in cubic perovskite materials. Cl- and Pb-based halide perovskite materials have the largest heavy, light and split-off electron effective masses. The results of our work may be expected to be useful in simulating the performance of perovskite-based opto-electronic devices.

VI. ACKNOWLEDGEMENT

The authors would like to thank Professor Walter R. L. Lambrecht and Dr. Ling-yi Huang for providing the data used to evaluate the Luttinger parameters of $CsBX_3(B = Pb, Si, Ge, X = Cl, Br, I)$ and Kane energy of of $CsBX_3(B = Sn, Si, Ge, X = Cl, Br, I)$.

VII. DATA AVAILABILTY STATEMENT

The data that supports the findings of this study are available within the article [and its supplementary material].

VIII. REFERNCES

[1] T. B. Bahder, Phys. Rev. B **41**, 11992 (1990).
[2] L. C. Lew Yan Voon and M. Willatzen, *The k p Method: Electronic Properties of Semiconductors*. (Springer, Berlin, 2009).
[3] J. Even, L. Pedesseau, J.-M. Jancu and C. Katan, Physica Status Solidi (RRL) **8**, 31 (2014).
[4] C. Zhang, D. Sun, C. X. Sheng, Y. X. Zhai, K. Mielczarek, A. Zakhidov and Z. V. Vardeny, Nat. Phys. **11**, 427 (2015).
[5] L.-y. Huang and W. R. L. Lambrecht, Phys. Rev. B **93**, 195211 (2016).
[6] H. Mehdizadeh-Rad and J. Singh, J. Appl. Phys. **126**, 153102 (2019).
[7] S. Ahmad, C. George, D. J. Beesley, J. J. Baumberg and M. De Volder, Nano Lett. **18** (3), 1856 (2018).
[8] N. Ashari-Astani, S. Meloni, A. H. Salavati, G. Palermo, M. Grätzel and U. Rothlisberger, J. Phys. Chem. C **121**, 23886 (2017).
[9] L.-y. Huang and W. R. L. Lambrecht, Phys. Rev. B **88**, 165203 (2013).
[10] D. Ompong and J. Singh, Org Electron. **63**, 104-108 (2018).
[11] H. Mehdizadeh-Rad and J. Singh, J. Mater. Sci. - Mater. Electron. **30**, 10064 (2019).
[12] L. D. Whalley, J. M. Frost, Y.-K. Jung and A. Walsh, J. Chem. Phys. **146**, 220901 (2017).
[13] P. Y. Yu and M. Cardona, *Fundamentals of Semiconductors: Physics and Materials Properties*, 4th ed. (Springer, Berlin, 2010).
[14] P. Azarhoosh, S. McKechnie, J. M. Frost, A. Walsh and M. v. Schilfgaarde, APL Mater. **4**, 091501 (2016).
[15] J. Singh and K. Shimakawa, *Advances in amorphous semiconductors*. (Taylor & Francis, London, 2003).
[16] J. Even, J. Phys. Chem. Lett. **6**, 2238 (2015).
[17] W. J. Fan, AIP Adv. **8**, 095206 (2018).
[18] M. A. Becker, R. Vaxenburg, G. Nedelcu, P. C. Sercel, A. Shabaev, M. J. Mehl, J. G. Michopoulos, S. G. Lambrakos, N. Bernstein, J. L. Lyons, T. Stöferle, R. F. Mahrt, M. V. Kovalenko, D. J. Norris, G. Rainò and A. L. Efros, Nat. **553**, 189 (2018).
[19] J. M. Luttinger, Phys. Rev. **102**, 1030 (1956).
[20] C. R. Pidgeon and R. N. Brown, Phys. Rev. **146**, 575(1966).
[21] Z. G. Yu, Sci. Rep. **6**, 28576 (2016).
[22] R. Ben Aich, S. Ben Radhia, K. Boujdaria, M. Chamarro and C. Testelin, J. Phys. Chem. Lett. **11**, 808 (2020).
[23] I. P. Pashuk, N. S. Pidzyrajlo and M. G. Matsko, Fizika Tverdogo Tela **23**, 2162 (1981).
[24] G. E. Eperon, S. D. Stranks, C. Menelaou, M. B. Johnston, L. M. Herz and H. J. Snaith, Energy Environ Sci. **7**, 982 (2014).
[25] V. V. Belykh, D. R. Yakovlev, M. M. Glazov, P. S. Grigoryev, M. Hussain, J. Rautert, D. N. Dirin, M. V. Kovalenko and M. Bayer, Nat. Commun. **10**, 673 (2019).

[26] C. Zhang, D. Sun, Z.-G. Yu, C.-X. Sheng, S. McGill, D. Semenov and Z. V. Vardeny, Phys. Rev. B **97**, 134412 (2018).